HTML ABSTRACT + LINKS

Remote quantitative temperature and thickness measurements of plasma-deposited titanium nitride thin coatings on steel using a laser interferometric thermoreflectance optical thermometer

Yue Liu, Andreas Mandelis,[a] Mervyn Choy, and Chinhua Wang
Department of Mechanical and Industrial Engineering, Center for Advanced Diffusion Wave Technologies, University of Toronto, 5 King's College Road, Toronto, Ontario M5S 3G8, Canada

Lee Segal
SPUTTEK Inc., 1 Goodmark Place, No. 4, Toronto, Ontario M9W 6M1, Canada

(Received 10 March 2005; accepted 20 June 2005; published online 3 August 2005)

An optical thermometer based on the principle of laser thermoreflectance has been introduced to monitor the surface temperature of thin coatings on steel parts undergoing an industrial titanium nitride (TiN) alloy deposition process. To study the feasibility of the optical thermometer, various thermo-optical parameters of TiN affected by the deposition process have been investigated; namely, the reflectance-temperature relation, the thermoreflectance coefficient, and the coating thickness dependence of thermoreflectance and of total reflectance. A theory of interferometric thermoreflectance has been introduced to model the total reflectance variations during the coating process. An inverse reflectance-temperature relation for the TiN–D2 steel substrate system has been found and a first-order Taylor series expansion used to model thermoreflectance has been shown to yield a thermoreflectance coefficient which is independent of temperature. Both results are in quantitative agreement with the Drude–Zener theory of conductors and semi-conductors. An empirical formula has been derived to effectively model the experimental thermoreflectance coefficient dependence of the TiN–D2 steel system on TiN coating thickness, in qualitative agreement with scattering mechanisms of the Boltzmann transport theory in conductors and semiconductors. The good agreement of theoretical interferometric thermoreflectance simulations with *in situ* measurements during a specific industrial TiN sputter-coating growth process and the independence of the thermoreflectance and thin-coating-thickness reflectance coefficients from temperature show the potential of using this nonintrusive noncontacting technique as an optical thermometer to determine surface temperatures of physically inaccessible samples undergoing industrial coating deposition processes. © *2005 American Institute of Physics.*
[DOI: 10.1063/1.2001673]

I. INTRODUCTION

There are many challenges in obtaining accurate surface temperature measurements under specific conditions during industrial alloy deposition processes. Underestimating the temperature commonly leads to overheating of metal parts within the alloy deposition chamber. As a result, undesired dimensional and property changes may occur. Likewise, overestimating temperatures leads to inhomogeneous surface coatings of insufficient quality and thickness. Therefore, a means to accurately determine the surface temperature of parts undergoing alloy deposition processes is of paramount importance.

A currently popular method of alloy deposition is by means of "sputtering." Sputtering chambers can reach temperatures of up to 400 °C through the use of radiant heaters under vacuum conditions. Furthermore, temperatures greater than 400 °C are attained by introducing argon plasma in the chamber. Many of these deposition chambers also incorporate rotating platforms as a method of depositing "target" coating material more uniformly onto the sputtered parts. Hostile conditions and/or ambients (e.g., low-pressure environments, high-temperature atmospheres, or rotating parts) that preclude the use of conventional contacting temperature sensors make it obvious that a noninvasive, remote method for measuring surface temperatures of coated components is required.

The most common commercial noncontact temperature measurement devices are pyrometers, also known as infrared or radiation thermometers. Despite their large success in providing noninvasive temperature measurements, pyrometers cannot be used under the conditions present in many alloy deposition chambers. Strong infrared radiation emission from radiant heaters and hot spots on parts being coated within those chambers tend to mask the emission from the observed surface. To overcome the problems, a remote temperature measurement technique based on laser thermoreflectance[1–4] has been developed. The technique of thermoreflectance which is based on the change of the refractive index of a material as a function of temperature (here

[a]Author to whom correspondence should be addressed; electronic mail: mandelis@mie.utoronto.ca

 © 2005 American Institute of Physics

Downloaded 18 Jul 2008 to 128.100.49.17. Redistribution subject to AIP license or copyright; see http://rsi.aip.org/rsi/copyright.jsp

also as a function of thin-layer thickness growth) has a strong potential for measuring temperature under hostile ambient conditions. The reflectivity of most dielectrics and metals in the visible spectral range is known to change proportionally with temperature.[5–7] By taking into account the surface condition of a material as well as the incident beam wavelength, angle, and polarization, a change in temperature can be related to the change in reflectivity. The most important issue with such a temperature measurement technique is to find the relationship between the reflectance and temperature variations, i.e., the thermoreflectance coefficient dR/dT, where R is the reflectance and T is the temperature. To the best of our knowledge, all previous reports have focused on the thermoreflectance coefficient study of homogeneous solid materials such as metals or semiconductors,[5,8,9] or semiconductors with dielectric transparent thin films[3,7,10] which are assumed to be nonabsorbing. However, in order to monitor the temperature variation during the coating process, knowing only the thermoreflectance coefficient of the substrate and of the coating materials is not enough. This is so because with the coating growing on top of the substrate, the initial reflectance of the substrate surface involves interferometric effects of a two-layer structure including substrate and thin coating. As a result, unlike the conventional thermoreflectance technique in which the total reflectance change from a surface of a homogeneous structure is solely due to the temperature change, the effect of the physical properties and the thickness of the growing thin film on the reflectivity must be considered. The total reflectance variation from such a two-layer substrate/thin coating system is due to two sources: One is caused by temperature change, which is conventionally called thermoreflectance variation, and is described by the thermoreflectance coefficient, dR/dT. The other source is the growing coating thickness, leading to related reflectance variations. The effect of thin-coating-thickness growth is described by the thin-coating-thickness reflectance coefficient, dR/dL, where L is the thickness of the thin film. Shen and Hua[11] measured the temperature of a transparent substrate during the vacuum evaporation of a transparent material coating through shifts of the optical interference fringes. Thermoreflectance and thin-coating-thickness reflectance (henceforth referred to as "interferometric thermoreflectance") are interrelated in the sputtering process and their combined effects on the total reflectance have not been studied to the best of our knowledge. In this article, a bulk conductor (metal) substrate and a thin-film system model will be presented describing the combined thin-coating-thickness reflectance and thermoreflectance phenomena from samples with D2 steel [a Fe alloy with a composition of C(1.5%), Cr (15.0%), Mo (1.0%), and V(1.0%)] as the substrate material and TiN as the coating material. The theoretical results have been applied to the temperature measurement during an industrial real-time TiN thin film deposition process.

II. THEORY OF BULK CONDUCTOR AND THIN CONDUCTING COATING THERMOREFLECTANCE

Reflectance is the ratio of reflected radiation power to incident power. Reflectivity is the intrinsic reflectance of a surface as a result of physical interactions between the incident radiation and the energetic structure of the irradiated medium, irrespective of geometric and source parameters such as sample thickness, growing surface layers, and irradiation power. The physical mechanism of thermoreflectance largely remains complicated and not fully understood in detail.[12] The complex index of refraction for most metals and dielectrics depends weakly on temperature,[2,5,10] resulting in a dependence of reflectivity, R, on temperature, T, according to the Fresnel formula of a vacuum-reflective material interface:

$$R(T) = \frac{[n(T)-1]^2 + k^2(T)}{[n(T)+1]^2 + k^2(T)}, \tag{1}$$

where n and k are the real and imaginary indices of refraction, respectively. The real and imaginary parts of the complex dielectric function ε of a solid can be expressed as combinations of n and k:

$$\varepsilon_1 = n^2 - k^2, \tag{2a}$$

$$\varepsilon_2 = 2nk, \tag{2b}$$

$$\varepsilon = \varepsilon_1 + i\varepsilon_2 = (n+ik)^2. \tag{2c}$$

Commonly k is referred to as the extinction coefficient. For small temperature changes resulting in small reflectivity changes, the phenomenon of thermoreflectance is linearized through a Taylor series expansion[13–15] as shown below:

$$R(T) = R(T_0) + \frac{dR}{dT}(T-T_0) + \frac{1}{2}\frac{d^2R}{dT^2}(T-T_0)^2 + \dots, \tag{3}$$

where T_0 is the ambient temperature. Through numerous independent studies,[6,13–15] the reflectivity, $R(T)$, has been found to be strongly dominated by the large invariant term, $R(T_0)$ and the small first-order term, $(dR/dT)\Delta T$, while higher order terms are negligible. Thus, the Taylor series expansion can be simplified:

$$\Delta R = R(T) - R_0 = \left(\left. \frac{dR}{dT} \right|_{T=T_0} \right) \Delta T. \tag{4}$$

The fractional reflectivity change from its value R_0 measured at the reference temperature, T_0, can be written

$$\frac{\Delta R}{R_0} = \frac{1}{R_0}\left(\left. \frac{dR}{dT} \right|_{T=T_0} \right) \Delta T \equiv \kappa \cdot \Delta T, \tag{5}$$

where the term $(1/R_0)(dR/dT)$ is commonly referred to as the linear thermoreflectance coefficient, κ (°C^{-1}). This coefficient can be treated as a constant by holding parameters such as surface conditions, wavelength, polarization, and incident angle constant.

For a bulk conducting substrate (metal or semimetal) the complex electrical conductivity can be expressed according to the Drude–Zener theory[16]

$$\sigma(\omega) = \frac{Ne^2\tau}{m^*(1-i\omega\tau)} \equiv \frac{\sigma_0}{1-i\omega\tau}, \tag{6}$$

where σ_0 is the dc electrical conductivity; N is the free-carrier density; m^* is the effective mass of free carriers in the medium; τ is the Boltzmann carrier relaxation (collision)

Downloaded 18 Jul 2008 to 128.100.49.17. Redistribution subject to AIP license or copyright; see http://rsi.aip.org/rsi/copyright.jsp

time constant following optical excitation; ω is the angular frequency of the electromagnetic (optical) field incident on the medium; and e is the elementary charge. The high-frequency complex dielectric function is related to $\sigma(\omega)$:

$$\epsilon(\omega) = \epsilon_0(\omega) + \left(\frac{4\pi i}{\omega}\right)\sigma(\omega) = (n + ik)^2, \tag{7}$$

where $\epsilon_0(\omega)$ is the contribution to $\epsilon(\omega)$ from all transport processes other than the free-carrier mechanism. Algebraic manipulation of Eqs. (2), (6), and (7) yields the following relations:

$$n^2 = \tfrac{1}{2}(\sqrt{\epsilon_1^2 + \epsilon_2^2} + \epsilon_1), \tag{8a}$$

$$k^2 = \tfrac{1}{2}(\sqrt{\epsilon_1^2 + \epsilon_2^2} - \epsilon_1), \tag{8b}$$

leading to the dependence of the reflectivity, Eq. (1), on the dielectric function

$$R(\epsilon_1, \epsilon_2) = \frac{(\epsilon_1^2 + \epsilon_2^2)^{1/2} + 1 - \sqrt{2}(\sqrt{\epsilon_1^2 + \epsilon_2^2} + \epsilon_1)^{1/2}}{(\epsilon_1^2 + \epsilon_2^2)^{1/2} + 1 + \sqrt{2}(\sqrt{\epsilon_1^2 + \epsilon_2^2} + \epsilon_1)^{1/2}}. \tag{9}$$

Typical values of relaxation time constants, τ, for several metals (e.g., Li, Na, Ag, Cu, Al) are in the range $(0.8–5.0) \times 10^{-14}$ s.[17] Introducing the free-carrier characteristic plasma frequency definition:

$$\omega_p = \sqrt{\frac{4\pi N e^2}{m^* \epsilon_0}} \tag{10}$$

with values $\sim(1–3)\times 10^{16}$ rad/s for typical metals,[18] it is concluded that for visible-spectral-range frequencies of the incident radiation, $\omega \sim 10^{15}$ rad/s, the following relations hold:

$$\omega\tau \gg 1, \quad \omega_p > \omega. \tag{11}$$

In this range of parameters, the reflectivity expression, Eq. (9), can be simplified using Eqs. (2c), (6), and (7) and the resulting approximations:

$$(\epsilon_1^2 + \epsilon_2^2)^{1/2} \approx \left(\frac{\omega_p}{\omega}\right)\left[1 + \frac{1}{2(\omega\tau)^2}\right] - 1, \tag{12}$$

$$n \approx \frac{1}{2}\left(\frac{\omega_p}{\omega^2 \tau}\right). \tag{13}$$

With these approximations we obtain

$$R(\tau) \approx 1 - \frac{2}{\omega_p \tau} + \left(\frac{1}{\omega_p \tau}\right)^2 \simeq 1 - \frac{2}{\omega_p \tau}. \tag{14}$$

Finally, from Eq. (6) R may be expressed in terms of the dc electrical conductivity of a conducting medium as a function of temperature

$$R(T) \approx 1 - 2\left[\frac{e^2 N(T)}{\omega_p m^* \sigma_0(T)}\right]. \tag{15}$$

Growing thin layers, which are different from the substrate material and are coated on a reflective surface, have been shown to greatly affect the total reflectivity, R, and the linear thermoreflectance coefficient, κ. As a result, the total reflectance and the linear thermoreflectance coefficient must be considered as a function of film or coating thickness, L. The relation between reflectance and coating thickness can be modeled in accordance with Fig. 1, where all three media (air, coating, and substrate) are assumed to be homogeneous. A plane wave can be resolved into two polarization components parallel (S) and perpendicular (P) to the plane of incidence. Usually each component has a different refection coefficient on the reflecting surface except in the special case of normal incidence. For simplicity, we only consider the P-polarization reflection coefficient as a function of arbitrary angle of incidence. It is easy to obtain a single polarization component beam in our experiments by introducing a linearly polarized laser beam to the experimental setup.

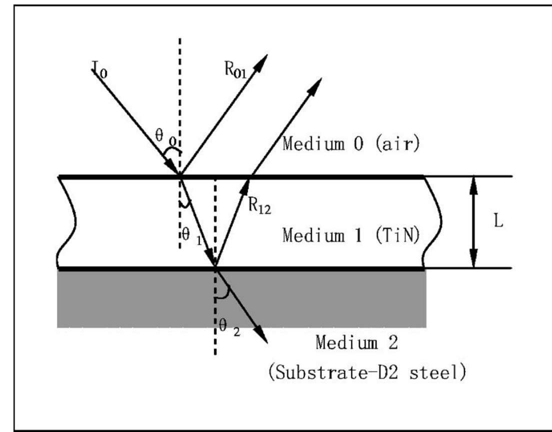

FIG. 1. Thin film model used to describe the effects of coating thickness on reflectance.

The general formula for two layer structure reflectance can be expressed as[19]

$$r = \frac{r_{01} + r_{12}e^{2i\beta L}}{1 + r_{01}r_{12}e^{2i\beta L}}, \tag{16}$$

where r_{01} and r_{12} are reflection coefficients of air-coating and coating-substrate interfaces, L is the thickness of the coating, and β is

$$\beta = \frac{2\pi}{\lambda}\bar{n}_1 \cos\theta_1. \tag{17}$$

Here $\bar{n}_1$ and θ_1 are refractive index of coating material and angle of refraction in medium 1, respectively. They can be real or complex depending on whether the coating is a dielectric or a conductor. Since the TiN coating grown on steel substrates and shown in Fig. 1 is a conducting material, both $\bar{n}_1$ and θ_1 are complex numbers. The same holds true for the steel substrate: $\bar{n}_2$ and θ_2 shown in Fig. 1 are complex numbers. It is convenient to set

$$\bar{n}_1 \cos\theta_1 = u_1 + i\nu_1,$$
$$\bar{n}_2 \cos\theta_2 = u_2 + i\nu_2, \tag{18}$$

u_1, ν_1 and u_2, ν_2 can be obtained as follows:

Downloaded 18 Jul 2008 to 128.100.49.17. Redistribution subject to AIP license or copyright; see http://rsi.aip.org/rsi/copyright.jsp

$$2u_j^2 = n_j^2 - k_j^2 - n_0^2 \sin^2\theta_0 + \sqrt{(n_j^2 - k_j^2 - n_0^2 \sin^2\theta_0)^2 + 4n_j^2k_j^2},$$
$$2\nu_j^2 = -[n_j^2 - k_j^2 - n_0^2 \sin^2\theta_0] + \sqrt{(n_j^2 - k_j^2 - n_0^2 \sin^2\theta_0)^2 + 4n_j^2k_j^2}, \tag{19}$$

where $j=1, 2$, n_0 is the refractive index of air or vacuum, and θ_0 is the angle of incidence. n_1, k_1 and n_2, k_2 are the real and imaginary indices of refraction of the thin coating and substrate, respectively. Then, the reflection coefficient of the P-polarized beam at the air-TiN interface can be written as[19]

$$r_{\perp 01} = \rho_{\perp 01}e^{i\phi_{\perp 01}} = \frac{n_0\cos\theta_0 - (u_1 + i\nu_1)}{n_0\cos\theta_0 + (u_1 + i\nu_1)}, \tag{20}$$

where

$$\rho_{\perp 01}^2 = \frac{(n_0\cos\theta_0 - u_1)^2 + \nu_1^2}{(n_0\cos\theta_0 + u_1)^2 + \nu_1^2},$$
$$\tan\phi_{\perp 01} = \frac{2\nu_1 n_0\cos\theta_0}{u_1^2 + \nu_1^2 - n_0^2\cos^2\theta_0}. \tag{21}$$

The reflection coefficient of the P-polarized beam at the TiN-steel interface can be written as

$$r_{\perp 12} = \rho_{\perp 12}e^{i\phi_{\perp 12}} = \frac{(u_2 + i\nu_2) - (u_1 + i\nu_1)}{(u_2 + i\nu_2) + (u_1 + i\nu_1)}, \tag{22}$$

where

$$\rho_{\perp 12}^2 = \frac{(u_2 - u_1)^2 + (\nu_2 - \nu_1)^2}{(u_2 + u_1)^2 + (\nu_2 + \nu_1)^2},$$
$$\tan\phi_{\perp 12} = \frac{2u_1\nu_2 - 2u_2\nu_1}{u_2^2 - u_1^2 + \nu_2^2 - \nu_1^2}. \tag{23}$$

Upon setting

$$\eta = \frac{2\pi}{\lambda_0} \tag{24}$$

and substituting $\rho_{01}, \phi_{01}, \rho_{12}, \phi_{12}, \eta$ from Eqs. (21), (23), and (24) in Eq. (10), the total reflectance R is given by

$$R = |r|^2 = \frac{\rho_{01}^2 e^{2\nu_1\eta L} + \rho_{12}^2 e^{-2\nu_1\eta L} + 2\rho_{01}\rho_{12}\cos(\phi_{12} - \phi_{01} + 2u_1\eta L)}{e^{2\nu_1\eta L} + \rho_{01}^2\rho_{12}^2 e^{-2\nu_1\eta L} + 2\rho_{01}\rho_{12}\cos(\phi_{12} + \phi_{01} + 2u_1\eta L)}. \tag{25}$$

The dependence of the linear thermoreflectance coefficient, κ, on the thickness, L, of the coating can be formally obtained using the following expression in the experimental results:

$$\kappa(L,T) = \frac{1}{R_0}\frac{\partial R(T,L)}{\partial T}. \tag{26}$$

The thin-coating-thickness reflectance coefficient, α, which is related to growing coating thickness changes can also be obtained in a similar manner:

$$\alpha(L,T) = \frac{1}{R_0}\frac{\partial R(T,L)}{\partial L}. \tag{27}$$

The reflectance contribution of the growing coating can be approximated using the first order Taylor series expansion for the reflectivity-temperature dependence. As a result, Eq. (5) can be generalized to include the first order dependence on thickness as well. Since the reflectivity is no longer that of a bulk conducting material (substrate), but instead, of a coating-substrate system, the total fractional reflectance $\Delta R/R_0$ is given by the interferometric thermoreflectance:

$$\frac{\Delta R(L,T)}{R_0} = \frac{R(T,L) - R(T_0,L_0)}{R_0} = \frac{1}{R_0}\frac{\partial R}{\partial L}\Delta L + \frac{1}{R_0}\frac{\partial R}{\partial T}\Delta T \equiv \alpha(L,T)\Delta L + \kappa(L,T)\Delta T, \tag{28}$$

where $\alpha(L,T)(\mathrm{m}^{-1})$ can be obtained formally by differentiating the effective reflectivity [Eq. (25)] with respect to the thin-film thickness, L.

III. MATERIALS AND SAMPLE PREPARATION

A set of steel samples were coated using a specific industrial TiN deposition process as described below. Each sample was a circular disc of AISI D2 steel. All samples were mirror polished to a degree required for industrial deposition processes.[20] The specific TiN coating process investigated in this work consists of five steps: vacuum preheating, argon plasma etching, target metal deposition, nitrogen plasma introduction, and recompression-cooling. Nitrogen plasma introduction is the controlled factor that is used to grow the TiN coating thickness. Each sample was mounted within a deposition chamber using identical mounting stands. The same chamber was used to coat all samples. Within the chamber, each sample was positioned in either one of two orientations. Samples “facing” the target flux tended to receive a more homogeneous and slightly thicker coating compared to those oriented “parallel” to the target flux for similar deposition processes. A description of the coating process for each sample is shown in Table I. All the coated samples were tested in a laboratory-based thermoreflectance setup to obtain the coefficient κ.

Downloaded 18 Jul 2008 to 128.100.49.17. Redistribution subject to AIP license or copyright; see http://rsi.aip.org/rsi/copyright.jsp

TABLE I. A description of the coating process for each sample.

Sample No.	Coating time (min)	Sample orientation
1	20	Parallel to target flux
2	30	Parallel to target flux
3	40	Parallel to target flux
4	25	Facing target flux
5	10	Facing target flux
6	18	Facing target flux
7	35	Parallel to target flux
8	35	Facing target flux polished

IV. EXPERIMENTAL SETUPS AND METHODOLOGY

The laboratory-based experimental setup, presented in Fig. 2(a), consists of a 10 mW, 632.8 nm linearly polarized He–Ne laser that serves as the probe light source. The emitted beam is mechanically chopped at 700 Hz and passes through a 380–780 nm polarizer to ensure linear polarization. The incident beam is then split into two beams using a cube beamsplitter, and the 90° reflected beam is focused onto a silicon photodiode connected to an EG&G 5210 lock-in amplifier referenced to the chopper frequency. The reflected beam is used to monitor laser power fluctuations. The forward transmitted beam continues on through a polarizing cube beam splitter (PCBS) aligned to the polarization of the incident beam, thus allowing for the majority of the incident beam to pass. The beam then traverses a 632 nm quarter-wave retardation plate which circularly polarizes the light. The circularly polarized beam is directed normal to the surface of the sample where it is reflected with the opposite direction of circular polarization. By optimizing the optical axis orientation of the quarter-wave plate (QWP), the reflected beam, upon passing again through the QWP, reemerges linearly polarized perpendicular to the polarization of the incident beam. As a result, the returning linearly polarized beam is redirected by the polarizing beamsplitter to the second silicon photodiode connected to another EG&G 5210 lock-in amplifier also referenced to the chopper frequency. The signals obtained by both lock-in amplifiers are recorded by a computer.

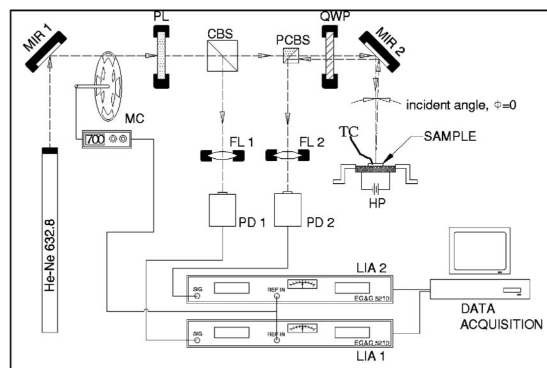

(a)

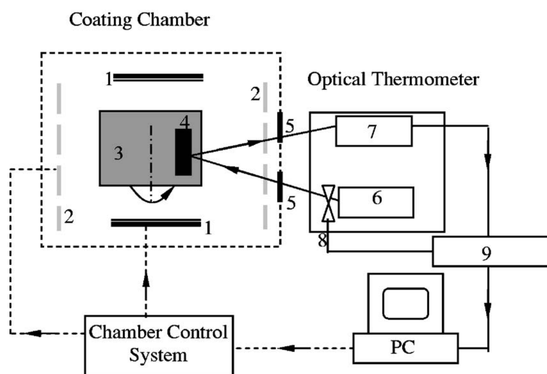

(b)

FIG. 2. (a) Laboratory experimental setup: (MIR) mirror, (PL) polarizer, (MC) mechanical chopper, (CBS) cube beamsplitter, (PCBS) polarizing cube beamsplitter, (QWP) quarter wave plate, (FL) focusing lens, (PD) photodiode, (HP) heater plate, (LIA) lock-in amplifier, and (TC) thermocouple. (b) Top-down view of the actual arrangements of the coating chamber and optical thermometer: (1) plasma bombarders, (2) radiation heaters, (3) sample holder, (4) sample, (5) observation windows, (6) linearly polarized laser, (7) photodiode, (8) mechanical chopper, and (9) lock-in amplifier.

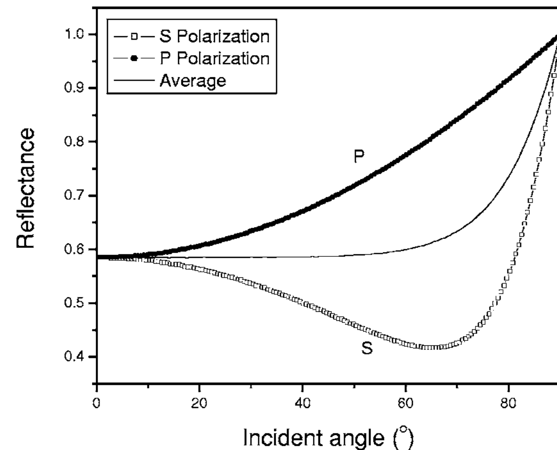

FIG. 3. The reflectance of a steel sample with refractive index $n=0.9$, $k=2.25$ under S,P, and averaged laser beam polarization.

The schematic of the experimental setup, installed at the level of the observation windows of the coating chamber acts as an optical thermometer, is shown in Fig. 2(b). The sample holder (No. 3) can rotate the sample if necessary, but measurements reported in this work were performed with stationary samples. The linearly polarized laser was rotated to generate a single polarization beam impinging on the sample inside the chamber. The laser beam from the optical system impinges onto the sample surface through one observation window and the reflected beam during the entire coating process is monitored by the photodiode (No. 7) through a second window adjacent to the entrance window. Since the incidence is not normal to the sample surface, the reflectances of the two polarization components are different. The theoretical perpendicular and parallel polarization reflectance of a steel sample with refractive index $n=0.9$, $k=2.25$[21] as a function of incident angle is shown in Fig. 3. It can be seen that the reflectance of the *P*-polarization component is larger than that of the *S*-polarization component for non-normal incidence. Based on these expectations, the linearly polarized laser beam was rotated to obtain maximum reflectance signal dominated by the *P*-polarized reflection during the *in situ* temperature measurements.

Changes in reflectance as a result of temperature variation were recorded with *ex situ* samples over relatively short

Downloaded 18 Jul 2008 to 128.100.49.17. Redistribution subject to AIP license or copyright; see http://rsi.aip.org/rsi/copyright.jsp

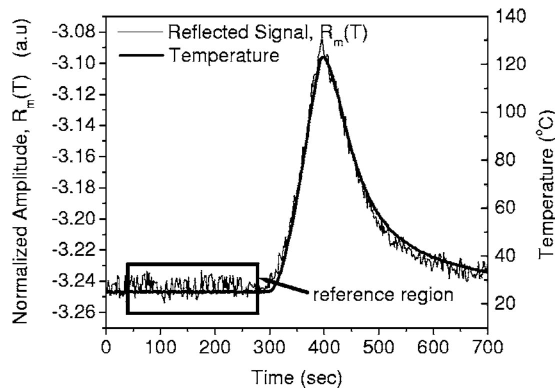

FIG. 4. Transient temperature and anticorrelated normalized reflectance amplitude of a TiN sample. The reference signal baseline is highlighted. Mean reference values were found to be T_o=25 °C, R_o=3.24 within the first 250 s. $R_m(T)$ is the reflectance signal normalized with the laser power. $-R_m(T)$ is plotted vs time in order to facilitate visual comparison of thermocouple and reflectance transients.

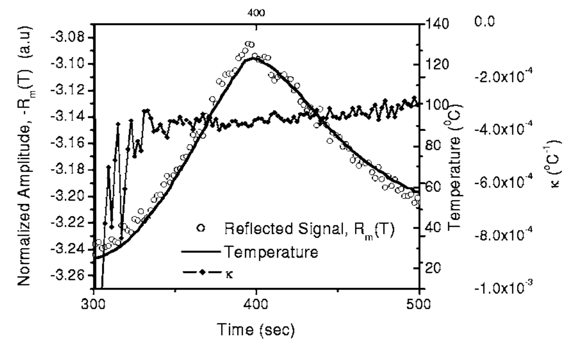

FIG. 5. Relative constancy of the thermoreflectance coefficient, κ, over the full rise and fall portion of the temperature cycle.

time periods (between 30 s and 1 min) using the setup of Fig. 2(a). This was accomplished by step-function powering of the heating plate on which the sample rested, and which had been preset to deliver the maximum power output. Fast activation of the heating plate allows for the highest possible rate of rise in sample surface temperature. Once the thermocouple read a surface temperature of approximately 120 °C, the heating plate was disconnected and a cooling fan was activated to air cool the sample. Step-function activation of the heating plate followed by fan cooling of the sample helps mitigate the formation of thermal gradients and hot stationary layers of the air above the sample surface. Thermal gradients in the air immediately above the sample result in varying densities which can create thermal profiles having different refractive indices. As a result, the reflected signal may be influenced not only by the surface-gas refractive index, but also by contributions of varying refractive indices brought upon by thermal gradients (thermal lensing). Therefore, by quickly increasing and decreasing the surface temperature, the relatively slowly evolving conductive air-heating effect was mitigated and its contribution was assumed to remain negligible on the time scale of our experiments.

The linear thermoreflectance coefficient was obtained using transient thermocouple and reflected optical signals normalized with respect to the laser power. For all experiments, a reference signal between 5 and 10 min was recorded before the temperature was increased. Typical experimental results from one coated sample with TiN coating and D2 steel substrate are shown in Fig. 4. During this initial reference period, the average reflectance and thermocouple readout temperature were calculated, thus establishing the reference reflectance, R_0, at the reference temperature, T_0. Knowledge of the reference reflectance, R_0, and temperature, T_0, allows the thermoreflectance coefficient, κ, to be determined for every instant by rearranging Eq. (4). The average thermoreflectance coefficient of the measurements shown in Fig. 4 is -3.12×10^{-4} °C^{-1}. Figure 5 proves that κ is relatively constant with respect to temperature essentially from the onset of heating and over the full heating and cooling cycle, in agreement with the underlying assumption in Eq. (4). Therefore, it was assumed that $\kappa(L,T)=\kappa(L)$ which was verified experimentally. The negative value of κ is consistent with the theoretical results predicted by Eq. (5), as well as with values reported in the literature.[22] The average thermoreflectance coefficient was thus recorded over the rise time and averaged.

The thin coating-thickness reflectance coefficient $\alpha(L,T)$ is a function of thin-film interferometric effects and initial and final optical states of the surface (initial: no coating, substrate reflectance only; final: fully opaque coating, coating reflectance only). The thickness growth rate is a complicated function of sputtering dynamics and substrate temperature. For simplicity, any temperature dependence of α can be incorporated in thickness variations and measured as thickness dependence. From this viewpoint, Eq. (27) leads to

$$\frac{\partial \alpha}{\partial T}=\frac{1}{R_0}\frac{\partial}{\partial T}\left[\frac{\partial R(L,T)}{\partial L}\right]=\frac{1}{R_0}\frac{\partial^2 R(L,T)}{\partial L^2}\frac{\partial L}{\partial T}. \tag{29}$$

In principle, the growth rate of coating thickness, L, depends on substrate temperature, T. However, the plasma deposition process which depends on several parameters such as plasma intensity, bias voltage, sample location, etc. is the major contributor in the TiN sputter-coating process and changes in sample temperature may not measurably affect the growth rate. Therefore, letting $\partial L/\partial T\sim 0$, gives $\partial\alpha/\partial T\sim 0$ in Eq. (29), i.e. $\alpha(L,T)\approx\alpha(L)$. This assumption is further supported by data in Fig. 12 to be discussed below.

Since the thin-coating-thickness reflectance coefficient is very sensitive to minute thickness changes contributing large optical interference variations to the measured reflectance, especially at the beginning of the thin-film growth range (<1 μm), a few reflection measurements at discrete thicknesses are not sufficient to accurately evaluate this coefficient as a function of the coating thickness L. This problem eventually disappears at long-time reflectance measurements during the coating process in which the coating thickness continually increases beyond the optically thick (opaque) range as determined by the optical absorption depth (inverse of the optical absorption coefficient at a given wavelength). Theoretical reflectance vs. thin-film thickness simulations using Eq. (25) with a D2 steel substrate (n_2=0.9 k_2=2.25) and three different coating materials with different optical properties at a constant temperature are shown in Fig. 6(a). Similar simulations involving the coefficient dR/dL are shown in

Downloaded 18 Jul 2008 to 128.100.49.17. Redistribution subject to AIP license or copyright; see http://rsi.aip.org/rsi/copyright.jsp

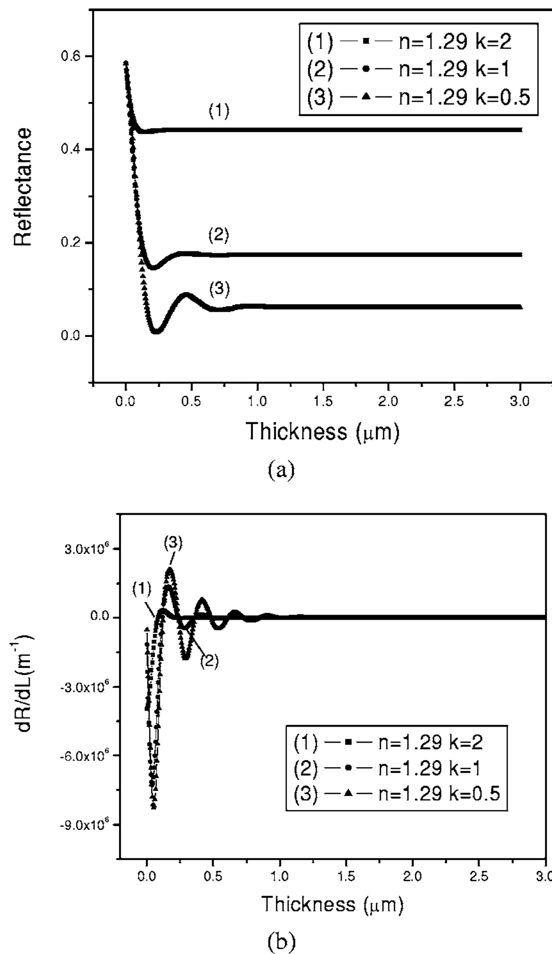

FIG. 6. Simulation results of: (a) R and (b) $\partial R/\partial L$ vs coating thickness with coating optical properties as parameters and fixed D2 steel substrate optical properties ($n_2=0.9$, $k_2=2.25$).

Fig. 6(b). The simulation results show that the interference patterns only exist within a very small coating thickness range when the extinction coefficient, k, is large. With k decreasing, the interference patterns become more pronounced and extend to a larger thickness range. Since it was hard to precisely control our industrial coating facility to prepare a series of uniformly coated samples with thin coating thicknesses within the interferometric range (from tens to hundreds of nanometers), it was found necessary to monitor the reflectance variation on one spot of a sample through the entire coating process, in which the coating thickness continually changed from 0 to several μm in order to test the theoretical predictions.

V. EXPERIMENTAL RESULTS AND DISCUSSION

It has been confirmed that the reflectance signal of each TiN coated steel sample decreases with increasing surface temperature. This type of inverse relationship between temperature and relative reflectance measurements of gold has also been observed by Claeys *et al.*[15] and by Decker and Hodgkin.[22] For very thin coatings below the optically thick limit (<1 μm) on bulk steel substrates, the substrate is expected to control both the temperature and the thermoreflectance behavior of the system. The temperature dependence of the free-carrier density, $N(T)$, can be ignored for relatively small temperature increases, such that the free-carrier kinetic energy change at the Fermi level is small:

$$\Delta\left(\frac{p_F^2}{2m^*}\right) \ll k_B(T-T_F)$$

or

$$\Delta p_F \sqrt{\frac{m^* k_B}{2T_F}} \ll \Delta T, \tag{30}$$

where T_F is the Fermi temperature, p_F is the free-carrier momentum at the Fermi level, and k_B is the Boltzmann constant. For most metals $T_F \sim O(10^4\ \mathrm{K})$,[23] which justifies ignoring the T dependence of N up to a few hundred °C. Therefore, the dominant temperature contribution to $R(T)$, Eq. (15), is through $\sigma_0(T)$. Differentiating Eq. (15) yields

$$\frac{\partial R(T)}{\partial T} = \left[\frac{2e^2N}{\omega_p m^* \sigma_0^2(T)}\right]\frac{\partial \sigma_0(T)}{\partial T}. \tag{31}$$

For temperatures well above the Debye temperature, Θ_D, of the substrate, it can be shown that the dc (or low-frequency) electrical conductivity is dominated by phonon scattering and it can be written as[18]

$$\sigma_0(T) = C\Theta_D^2/T; T \geq 0.2\ \Theta_D, \tag{32}$$

where C is a temperature-independent constant. Even though Θ_D for D2 steel composition is unknown, nevertheless, for Fe the Debye temperature is 460 K (187 °C). Therefore, the temperature range spanned in the measurements of Figs. 4 and 5 is in the $T \geq 0.2\ \Theta_D$ regime and Eq. (32) is very likely valid for D2 steel as well. Inserting Eq. (32) into Eq. (31) yields

$$\frac{\partial R(T)}{\partial T} = -\frac{2e^2N}{\omega_p m^* C\Theta_D^2}\ (\text{independent of } T). \tag{33}$$

For Ag, Cu, and Al the right-hand-side of Eq. (33) can be calculated to be in the range of -1.4×10^{-5} and $-1.7\times10^{-5}\ ^\circ\mathrm{C}^{-1}$.[22] The value of κ obtained from the TiN–D2 sample (Fig. 5) is one order higher than these theoretically calculated values. In order to test the reliability of our thermoreflectance measurement methodology, a reference Si wafer sample was tested and compared to thermocouple readings with the setup of Fig. 2(a). We obtained $\kappa=1.44\times10^{-4}\ \mathrm{C}^{-1}$, which is well within the range of the published values of $1.2\times10^{-4}\ \mathrm{K}^{-1}$ 4 and $1.6\times10^{-4}\ \mathrm{K}^{-1}$.[24] This agreement of our results with literature values for κ assures the reliability and quantitative capabilities of our instrumental setup.

The independence of κ from T above 70–80 °C in Fig. 5 shows that the high-temperature approximation for the bulk substrate D2 steel conductivity, Eq. (32), is also valid for the TiN–D2 steel system. The fact that κ is independent of T is important as it renders the instrumental implementation of the interferometric thermoreflectance technique feasible toward a noncontacting quantitative optical thermometer.

A. Thin-coating-reflectance coefficient, $\alpha(L)$

The thin-coating-thickness reflectance coefficient, α, was defined in Eq. (27) as the proportionality coefficient be-

Downloaded 18 Jul 2008 to 128.100.49.17. Redistribution subject to AIP license or copyright; see http://rsi.aip.org/rsi/copyright.jsp

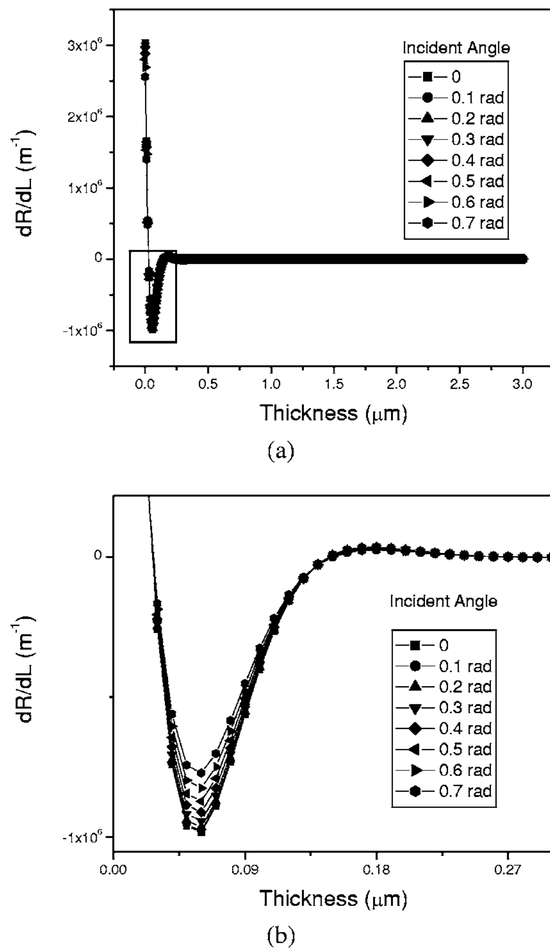

FIG. 7. (a). Simulation of thin-coating-thickness reflectance coefficient dR/dL of a two-layer system with constant temperature and reference optical values (vacuum: $n_0=1$, $k_0=0$; TiN: $n_1=1.29$, $k_1=2.76$; D_2 steel: $n_2=0.9$, $k_2=2.25$), P polarization, and various incident angles. (b) Magnification of the region within the box shown in (a).

tween varying reflectance and coating thickness growth, ΔL. This coefficient can be obtained by differentiating the total reflectance [Eq. (25)] with respect to thickness, L. The plots of the theoretical $\alpha(L,T_o)$ of the TiN–D2 steel two-layer structure with reference optical property values (vacuum: $n_0=1$, $k_0=0$; TiN: $n_1=1.29$, $k_1=2.76$;[25] steel: $n_2=0.9$, $k_2=2.25$),[21] P-polarization incident beam and various incident angles versus coating thickness are shown in Fig. 7. They illustrate that for thicknesses <0.3 μm, the contribution of coating thickness to the reflectance is significant. Because the minimum of $\partial R/\partial L$ is on the order of -10^6 m^{-1} and coating thicknesses are on the order of 10^{-8}–10^{-7} m, the thin-coating-thickness reflectance contribution, $(\partial R/\partial T)\Delta L$, is on the order of 10^{-2}–10^{-1}. Since most thermoreflectance coefficients, κ, are on the order of 10^{-5}–10^{-4} °C^{-1}[26] and temperature changes during the industrial deposition process are on the order of 10^2 °C, it follows that dominant contributions to the full reflectance resulting from film growth are expected only for thicknesses $L<0.3$ μm. At coating thicknesses above 0.3 μm, $\partial R/\partial L$ essentially becomes 0, implying total opacity of the TiN coating. As a result, coating growth beyond 0.3 μm does not contain thickness-reflectance information. Furthermore, the plots show that the interference minimum is essentially independent of the angle and the state of polarization.

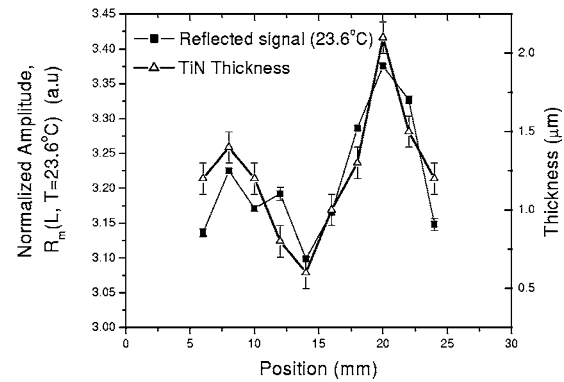

FIG. 8. Comparison of reflectance measurements at room temperature with thickness of sputter-coated TiN layers.

B. Thickness dependence of the thermoreflectance coefficient, $\kappa(L)$

As discussed in Sec. IV, experimentally shown in Fig. 5, and theoretically established through Eq. (33), the thermoreflectance coefficient is only a function of coating thickness and not of temperature. To determine this function, one sample (No. 7) was selected to perform thickness-reflectance measurements as a result of exhibiting visual variations in coating thickness across the surface, resulting from a nonhomogeneous TiN deposition process. Before the sample was cross sectioned for coating thickness measurements, thermoreflectance measurements on different spots of a cross-sectional line which covers a visually inhomogeneous range were performed. For each coordinate point measurement, the sample was heated to 120 °C and subsequently cooled to room temperature, while the reflectance signals throughout the entire heating and cooling process were recorded. Using the methodology of Sec. IV, we obtained a series of thermoreflectance coefficients. Then, a Hitachi S-2500 tungsten filament scanning electron microscope was employed to measure the variable coating thickness.

The comparison of the average reflectance value at room temperature with the thickness measured at the same spots, Fig. 8, shows that there is a strong proportional correlation between reflectance and coating thickness beyond the optical interference saturation limit. Therefore, this correlation can be used as a nondestructive technique to test the homogeneity of the coated samples when the coating thickness is too thin (from sub μm to a few μm) for other techniques, such as thermal waves, to be sensitive in this thickness range. Figure 9 shows a room temperature reflectance image of a mildly inhomogeneous TiN–D2 steel sample. It can be concluded that interferometric thermoreflectance scanning can be used to monitor coating homogeneities during or after the coating process. The technique is based on the variation of the thermoreflectance coefficient κ with coating thickness L. A quantitative comparison of the experimental thermoreflectance coefficient with thickness measured at the same spots exhibited a decreasing trend in κ, with L. This trend is best shown using a logarithmic fit, Fig. 10. The logarithmic fit is

Downloaded 18 Jul 2008 to 128.100.49.17. Redistribution subject to AIP license or copyright; see http://rsi.aip.org/rsi/copyright.jsp

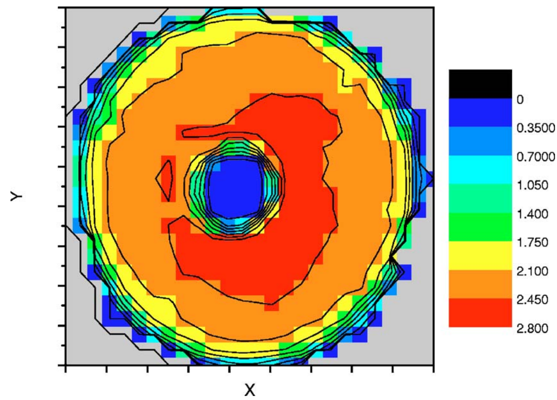

FIG. 9. (Color online) Reflectance image of an ultrathin mildly inhomogeneous sample at room temperature. Thickness range: 0.35–2.80 μm. Image profiles correlate with thickness inhomogeneity profiles.

employed to optimize the sensitivity of modeling the saturation limit of the thermoreflectance coefficient with increasing coating thickness. As discussed above, at thicknesses above the optically thick limit, the coating becomes totally opaque and the reflectance is strictly based on the solid-state properties of the coating and on its temperature, which is controlled by substrate heat conduction. The saturation limit for TiN lies between $-3\cdot 10^{-4}$ and $-2\cdot 10^{-4}\ ^\circ\mathrm{C}^{-1}$, values also supported by other experimental results showing that the coefficient of thermoreflectance is approximately $-2.43\cdot 10^{-4}\ ^\circ\mathrm{C}^{-1}$ for a fully opaque coated sample. The best fit to the data shown in Fig. 10 resulted in the following empirical relation:

$$\kappa(L) = -0.00011 - 0.00019\ln(L+0.5)^\circ\mathrm{C}^{-1}, \tag{34}$$

where L is the coating thickness in μm. Since the sample was prepared with industrial equipment, the quality was not as tightly controlled as may have been expected. The coating inhomogeneity caused by the coating process certainly has introduced error to our experimental results, as shown by the large deviations between the theoretical curve and experimental results in Fig. 10. However, at each point the error bars are no worse than those shown in Fig. 8 and the decreasing trend in the mean is obvious. Our choice of a logarithmic relationship was driven by the need to amplify and highlight

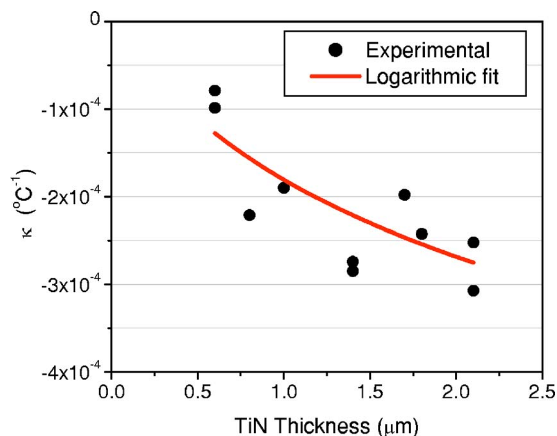

FIG. 10. (Color online) Thermoreflectance coefficient vs TiN thickness measurements and best fitted decreasing logarithmic relation, Eq. (34).

the relatively weak dependence of thermoreflectance coefficient on thickness. The decreasing trend of the coefficient $\kappa(L)=(1/R_0)[\partial R(L)/\partial T]$ with coating thickness, L, is as expected from the Boltzmann transport equation.[18] While boundary and defect scattering mechanisms in bulk conducting and semiconducting solids, at temperatures higher or commensurate with the range of the Debye temperature, are secondary to electron-phonon scattering which gives rise to the expression for the dc conductivity described by Eq. (32), these mechanisms become important with increased confinement of free carriers, such as in the case of thin films and coatings. These additional scattering degrees of freedom impact the overall relaxation (collision) time τ, the sum of all collisional rates:

$$\frac{1}{\tau} = \sum_i \frac{1}{\tau_i}. \tag{35}$$

The presence of discrete interfaces (surfaces) of the coating amounts to efficient carrier traps; for thickness L one expects $\tau(L) < \tau(\infty)$. Therefore, from the definition of σ_0:

$$\sigma_0(L) = \left(\frac{e^2 N}{m^*}\right)\tau(L) < \sigma_0(\infty), \tag{36}$$

or, equivalently, from Eqs. (32) and (36)

$$C(L)/C(\infty) = \tau(L)/\tau(\infty) < 1. \tag{37}$$

Finally, Eq. (33) gives

$$\frac{\partial R(T,L)}{\partial T} = \frac{\partial R(T,\infty)}{\partial T}\left[\frac{\tau(L)}{\tau(\infty)}\right]. \tag{38}$$

Hence, as $\tau(L)$ increases with increasing coating thickness, owing to the receding interfaces and perhaps a decrease in the mechanical defect density which acts as free-carrier traps, $\partial R(T,L)/\partial T$ is expected to increase in magnitude as observed in Fig. 10. Equation (34) can be used, in principle, to describe the relaxation time variation with coating thickness. The change in $\tau(L)$ is expected to saturate at the bulk value of the coating material as the thickness becomes much larger than the mean scattering length l. Unfortunately, the values of these statistical parameters are not known for TiN.

C. Total reflectance measurements of temperature by the optical thermometer

As discussed in Sec. II, the overall reflectance of a composite-layer solid with a thin-film layer can be approximated using a first order Taylor series expansion in terms of coating thickness and temperature as shown in Eq. (28). In order to explicitly determine the temperature dependence of the reflectance signal, ΔR, knowledge of the thin-coating-thickness reflectance coefficient, $\alpha(L)$, of the linear thermoreflectance coefficient, $\kappa(L)$, and of the coating thickness, ΔL, is required. So far it has been established that α and κ can be given as explicit functions of coating thickness, L. Therefore, Eq. (28) may be used to resolve the temperature-reflectance relationship, provided the coating thickness can be determined independently of the reflectance. This can be done by developing a calibration curve of the industrial sputtering growth process by carefully measuring surface layer thickness versus deposition time. Once the thickness is

Downloaded 18 Jul 2008 to 128.100.49.17. Redistribution subject to AIP license or copyright; see http://rsi.aip.org/rsi/copyright.jsp

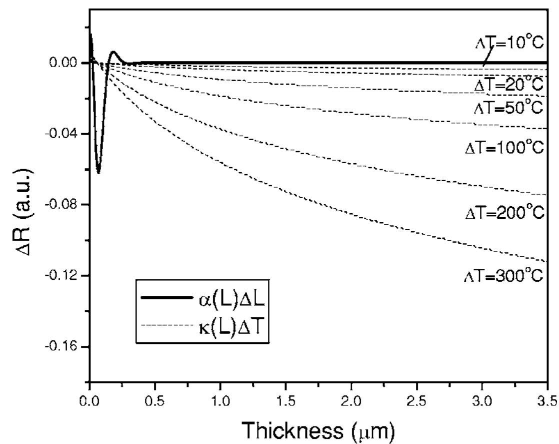

FIG. 11. Theoretical ΔR contributions of $\alpha(L)\Delta L$ and $\kappa(L)\Delta T$ for various thicknesses and temperatures.

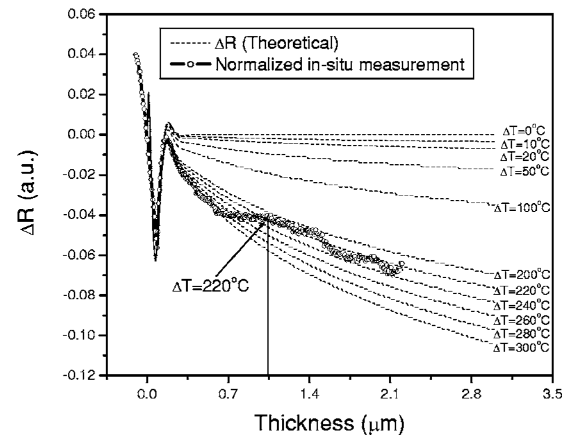

FIG. 12. Comparison of theoretical ΔR based on Eq. (28) for various thicknesses and temperatures under real-time *in situ* sputter-coating process monitoring.

known, $\alpha(L)$ and $\kappa(L)$ can be obtained using the thickness derivatives of Eqs. (25) and (34), respectively. With known $L, \alpha(L), \kappa(L)$, and the measured reflectance signal, ΔR, Eq. (25) can be used to solve for the surface temperature ΔT.

The contribution of each reflectance constituent, $\kappa(L)\Delta T$, and $\alpha(L)\Delta L$ varies depending on both changes in temperature and thickness. Figure 11 shows theoretical dependencies of $\alpha(L)$ and $\kappa(L)$ on coating thickness using the thickness derivatives of Eqs. (25) and (34). As discussed in Sec. V, the contribution of $\alpha(L)\Delta L$ totally dominates the reflectance signal in the thickness range below 0.3 μm, theoretically validating the assumption $\alpha=\alpha(L)$ (independent from T). The locations of the interference extrema depend on the optical properties of both coating and substrate materials. Once the properties of the coating and substrate materials are known, the extrema appear at fixed thicknesses. The large inverted peak shown in Fig. 11 can be a useful feature toward determining the coating thickness essentially at the beginning of the coating process (a time thickness marker for the later growth of the coating). However, at larger thicknesses $(\Delta L > 0.3\ \mu\text{m}), \alpha(L)$ approaches 0 and the change in reflectance signal is dominated by the change in temperature. Therefore, the contribution of each reflectance parameter, $\kappa(L)\Delta T$, and $\alpha(L)\Delta L$ will depend on interdependent changes in coating thickness and temperature. Figure 12 shows the theoretical total reflectance variation (ΔR) by combining $\kappa(L)\Delta T$, and $\alpha(L)\Delta L$, together with one normalized interferometric thermoreflectance measurement result using the setup in Fig. 2(b). As expected, the interference pattern occurs at thicknesses $<0.3\ \mu$m and it is essentially the same for all T, thus also validating experimentally the assumption $\alpha=\alpha(L)$. At thicknesses $>0.3\ \mu$m, the signal switches between two curves with $\Delta T=200$ and 300 °C. This means that, compared to the onset temperature of the coating process (usually around 350 °C), the temperature increased ~200–220 °C at later times, corresponding to $\Delta L > 1\ \mu$m. This temperature determination is in agreement with the thermocouple temperature readings. Using this optical thermometer to measure the temperature at a certain coating thickness, one can easily draw a vertical line from a thickness point and find the intersection of the experimental data and the theoretical isotherm. According to the example shown in Fig. 12, at the thickness of 1 μm, the experimental curve coincides with the theoretical isotherm at 220 °C. This can be taken to be the coating surface temperature when the thickness is 1 μm. The experimental curve further reveals relatively large temperature fluctuations between 200 and 300 °C during the entire 2.5 μm coating growth cycle.

In summary, it is concluded that the interferometric thermoreflectance technique presented here amounts to an optical thermometer, owing to the independence of the coefficients κ and α from temperature, at least within the ranges of the reported experiments. The thermometer was developed to monitor the surface temperature of steel parts with a growing thin coating, the result of an industrial titanium nitride (TiN) alloy deposition process. The thermoreflectance coefficient, the thin-coating-thickness reflectance coefficient, and the contribution of these two factors to the total reflectance variation of TiN were investigated experimentally and theoretically to study the feasibility of the optical thermometer. The investigation revealed an inverse reflectance-temperature relation for the TiN–D2 steel system, in agreement with the Drude–Zener theory. A total reflectance theory based on a first order Taylor series expansion of the film thickness and temperature-dependent reflectivity function was introduced. The thermoreflectance coefficient, $\kappa(L)$ for TiN-coated steel samples was found to decrease (absolute value increased) with increasing TiN coating thickness, in qualitative agreement with the Boltzmann transport theory. The thin-coating-thickness reflectance coefficient, $\alpha(L)$, was determined from the thickness derivative of the total reflectance. The question of the dominant contribution to ΔR by either $\alpha(L)\Delta L$ or $\kappa(L)\Delta T$ terms was shown to depend on the coating thickness and temperature changes for different thickness regions. For TiN coating thicknesses greater than 0.3 μm, the change in reflectance is dominated by $\kappa(L)\Delta T$. The excellent agreement between the reflectance and thermocouple results for a specific industrial sputtering TiN-deposition process has confirmed the feasibility of the optical thermometer in the configuration of Fig. 2(b). This instrument has the potential of employing the combined optical interferometric and temperature dependent reflectance of

Downloaded 18 Jul 2008 to 128.100.49.17. Redistribution subject to AIP license or copyright; see http://rsi.aip.org/rsi/copyright.jsp

surface-coated solids to determine surface temperatures of manufactured parts with growing thin coatings in a remote, nonintrusive manner.

ACKNOWLEDGMENTS

The authors gratefully acknowledge Materials and Manufacturing Ontario for a Collaborative contract with Sputtek Inc., which made this research possible.

[1] D. J. Price, Proc. Phys. Soc. London **59**, 131 (1947).
[2] C. H. Fan and J. P. Longtin, Exp. Therm. Fluid Sci. **23**, 1 (2000).
[3] V. Quintard, G. Deboy, S. Dilhaire, D. Lewis, T. Phan, and W. Claeys, Microelectron. Eng. **31**, 291 (1996).
[4] G. E. Jellison and H. H. Burke, J. Appl. Phys. **60**, 841 (1986).
[5] A. S. Lee and P. M. Norris, Rev. Sci. Instrum. **68**, 1307 (1997).
[6] G. E. Jellison and F. A. Moine, Phys. Rev. B **27**, 7466 (1993).
[7] D. Guidotti and J. G. Wilman, J. Vac. Sci. Technol. A **10**, 3184 (1992).
[8] H. Kempkens, W. W. Byszewski, P. D. Gregor, and W. Lapatovich, J. Appl. Phys. **67**, 3618 (1990).
[9] V. Quintard, S. Dilhaire, T. Phan, and W. Claeys, IEEE Trans. Instrum. Meas. **48**, 69 (1999).
[10] J. Heller, J. W. Bartha, C. C. Poon, and A. C. Tam, Appl. Phys. Lett. **75**, 43 (1999).
[11] Y. H. Shen and C. Y. Hua, Nucl. Instrum. Methods **167**, 139 (1979).
[12] F. Abeles, *Optical Properties of Solids* (North-Holland, Amsterdam, 1972), pp. 257–261.
[13] N. Araki, D. W. Tang, and H. Kawashima, Int. J. Thermophys. **23**, 245 (2002).
[14] D. Guidotti and J. G. Wilman, Appl. Phys. Lett. **60**, 524 (1992).
[15] W. Claeys, S. Dilhaire, S. Jourez, and L. D. Pantino-Lopez, Microelectron. J. **32**, 891 (2001).
[16] W. Jones and N. H. March, *Theoretical Solid State Physics*, Vol. 2, Non-equilibrium and Disorder (Dover, New York, 1973), Chap. 7.2.
[17] A. J. Dekker, *Solid State Physics* (Prentice-Hall, Englewood Cliffs, NJ, 1954).
[18] J. M. Ziman, *Principles of the Theory of Solids* (Cambridge University Press, Cambridge, 1972), Chaps. 7 and 9.
[19] M. Born and E. Wolf, *Principles of Optics*, 6th ed. (Pergamon, Oxford, 1980), Chaps. 1, 7, 13.
[20] Sputtek Inc. Toronto, On, CANADA ⟨http://www.sputtek.com⟩
[21] S. Nolte, Appl. Phys. A: Mater. Sci. Process. **68**, 563 (1999).
[22] D. L. Decker and V. A. Hodgkin, *Proceedings, Symposium on Laser Induced Damage in Optical Materials*, Boulder, CO, 30 September–1 October 1980 (National Bureau of Standards, Washington, D.C., 1981), p. 190.
[23] C. Kittel, *Thermal Physics* (Wiley, New York, 1969), p. 236.
[24] A. Mandelis and R. E. Wagner, Jpn. J. Appl. Phys., Part 1 **35**, 1786 (1996).
[25] E. D. Palik, *Handbook of Optical Constants of Solids II* (Academic, San Diego, 1991), pp. 117–201, 307.
[26] A. Rosencwaig, J. Opsal, W. L. Smith, and D. L. Willenborg, Appl. Phys. Lett. **46**, 1013 (1985).

Downloaded 18 Jul 2008 to 128.100.49.17. Redistribution subject to AIP license or copyright; see http://rsi.aip.org/rsi/copyright.jsp